

The bright optical/NIR afterglow of the faint GRB 080710 - Evidence for a jet viewed off axis

T. Krühler^{1,2}, J. Greiner¹, P. Afonso¹, D. Burlon¹, C. Clemens¹, R. Filgas¹, D. A. Kann³, S. Klose³, A. Küpcü Yoldaş⁵, S. McBreen⁴, F. Olivares¹, A. Rau¹, A. Rossi³, S. Schulze^{3,6}, G. P. Szokoly⁷, A. Updike⁸, and A. Yoldaş¹

¹ Max-Planck-Institut für extraterrestrische Physik, Giessenbachstrasse, 85748 Garching, Germany. e-mail: kruehler@mpe.mpg.de

² Universe Cluster, Technische Universität München, Boltzmannstrasse 2, 85748 Garching, Germany.

³ Thüringer Landessternwarte Tautenburg, Sternwarte 5, 07778 Tautenburg, Germany

⁴ School of Physics, University College Dublin, Dublin 4, Ireland

⁵ European Southern Observatory, 85748 Garching, Germany.

⁶ Center for Astrophysics and Cosmology, University of Iceland, Dunhagi 5, 107 Reykjavík, Iceland

⁷ Institute of Physics, Eötvös University, Pázmány P. s. 1/A, 1117 Budapest, Hungary

⁸ Department of Physics and Astronomy, Clemson University, Clemson, SC 29634, USA.

ABSTRACT

Aims. We investigate the optical/near-infrared light curve of the afterglow of GRB 080710 in the context of rising afterglows.

Methods. Optical and near-infrared photometry was performed using the seven channel imager GROND and the Tautenburg Schmidt telescope. X-ray data were provided by the X-ray Telescope onboard the *Swift* satellite. We construct an empirical light curve model using the available broadband data, which is well-sampled in the time and frequency domains.

Results. The optical/NIR light curve of the afterglow of GRB 080710 is dominated by an initial increase in brightness, which smoothly turns over into a shallow power law decay. At around 10 ks post burst, there is an achromatic break from shallow to steep decline in the afterglow light curve with a change in the power law index of $\Delta\alpha \sim 0.9$.

Conclusions. The initially rising achromatic light curve of the afterglow of GRB 080710 can be accounted for with a model of a burst viewed off-axis or a single jet in its pre deceleration phase and in an on-axis geometry. A unified picture of the afterglow light curve and prompt emission properties can be obtained with an off-axis geometry, suggesting that late and shallow rising optical light curves of GRB afterglows might be produced by geometric effects.

Key words. gamma rays: bursts

1. Introduction

The launch of the *Swift* satellite (Gehrels et al. 2004) in 2004 opened a new field of Gamma-Ray Burst (GRB) afterglow physics. With its precise localization by the Burst Alert Telescope (BAT; Barthelmy et al. 2005), rapid slewing capabilities and early follow up with two instruments in the X-ray and ultraviolet/optical regime, studies of the early afterglow phase were possible for the first time with larger sample statistics of around 50 per year.

Long GRBs are generally classified according to the spectral properties of their prompt emission. While conventional GRBs (CGRBs) have the peak energy of their observed spectrum in the 300 keV range (Preece et al. 2000), the spectrum of X-ray rich bursts (XRRs) and X-ray flashes (XRFs) peak at significantly lower energies, typically around 50 keV for XRRs or 10 keV for XRFs respectively (e.g. Heise et al. 2001; Kippen et al. 2003). The spectral and temporal properties (e.g. Sakamoto et al. 2005) and their similar afterglows as compared to CGRBs provide strong evidence, though, that XRRs/XRFs represent a softer region of a continuous GRB distribution (e.g. Lamb et al. 2005; Sakamoto et al. 2008).

An unified picture of the subclasses of GRBs can be obtained when attributing the observed differences in their peak energy to different angles with respect to the symmetry axis of the jet (e.g. Yamazaki et al. 2002). The kinetic energy in the jet per solid angle ε is usually parametrized as

a top hat (e.g. Rhoads 1999; Woods & Loeb 1999), Gaussian (Zhang & Mészáros 2002), power law structured outflow with $\varepsilon \propto (\theta/\theta_{jet})^{-q}$ (Mészáros et al. 1998), or a top hat with lower energetic wings. The resulting shape of the afterglow light curve then depends on the viewing angle and jet structure (e.g. Rossi et al. 2002).

In an inhomogeneous jet model, the initial bulk Lorentz factor as well as the specific deceleration time and radius are dependent on the distance to the symmetry axis of the jet (Kumar & Granot 2003). Hence, a geometric offset of the observers line of sight from the jets symmetry axis will have a distinct signature in the optical light curve (e.g. Granot & Kumar 2003). Due to the relativistic beaming of the decelerating ejecta, an observer located off-axis to the central jet will see a rising optical afterglow light curve at early times (e.g. Panaitescu et al. 1998; Granot et al. 2002). The steepness of the rise would then be characteristic of the off-axis angle and the jet structure: the farther the observer is located from the central emitting cone or the faster the energy per solid angle decreases outside the jet, the shallower is the observed rise in a structured jet model (Panaitescu & Vestrand 2008). A restframe peak energy E_{peak}^{rest} consistent with an XRF would thus correspond to a shallow rise or early plateau phase of the afterglow. With decreasing off-axis angle, both E_{peak}^{rest} and the optical afterglow rise index will increase to XRRs and steeper rising early afterglow light curves.

2. Observations

At $T_0=07:13:10$ UT on 10 July 2008, *Swift* triggered and located GRB 080710, but did not slew immediately to the burst (Sbarufatti et al. 2008). Due to an observing constraint, observations with the two narrow field instruments, the X-ray (XRT; Burrows et al. 2005) and UV/Optical Telescope (UVOT; Roming et al. 2005) started 0.87 h and 0.89 h after the trigger (Landsman & Sbarufatti 2008). The burst had a relatively smooth fast rise - exponential decay structure with $T_{90}(15-350 \text{ keV}) = 120 \pm 17 \text{ s}$ and weak indication of a precursor 120 s before the main peak (Tueller et al. 2008). Above 100 keV, the burst is only marginally detected by BAT and its spectrum is well described with a single power law of index -1.47 ± 0.23 with a total fluence in the 15-150 keV range of $1.4 \pm 0.2 \cdot 10^{-6} \text{ erg/cm}^2$ (Tueller et al. 2008). Using the spectral slope from the BAT data, and following Sakamoto et al. (2009), the peak energy of the prompt emission spectrum can be constrained to $110^{+340}_{-60} \text{ keV}$ including the uncertainties of the BAT power law slope. The fluence ratio of GRB 080710 between the two BAT bands 25-50 keV and 50-100 keV is $S(25-50 \text{ keV})/S(50-100 \text{ keV}) = 0.70 \pm 0.15$, and the burst thus qualifies as a CGRB in the observers frame, with errors ranging into XRRs when applying the working definition of Sakamoto et al. (2008).

Assuming a spectral shape of a Band function (Band et al. 1993) with a peak energy of around 110 keV and a high energy index of -2.5 , standard Λ CDM cosmology ($\Omega_M=0.27$, $\Omega_\Lambda=0.73$, $H_0=71 \text{ (km/s)/Mpc}$) and a redshift of 0.845 (Perley et al. 2008; Fynbo et al. 2009) we derive a bolometric energy release for GRB 080710 of $\log E_{\gamma, \text{iso}}[\text{erg}] = 51.75$ with a restframe peak energy of $E_{\text{peak}}^{\text{rest}} \sim 200 \text{ keV}$. Peak energies of the observed prompt spectrum of 50 keV, 300 keV or 500 keV result in $\log E_{\gamma, \text{iso}}[\text{erg}] \approx 51.70, 51.94$ or 52.14 , respectively. Compared to a sample of previous bursts with known redshift (e.g. Amati et al. 2008), these estimates put GRB 080710 to the lower energy end of GRBs, with an inferred bolometric energy release of around 10^3 times less than the extremely energetic GRB 080916C (Abdo et al. 2009; Greiner et al. 2009a). Hence, a low $E_{\text{peak}}^{\text{rest}}$ in the 50-200 keV range is also supported by the Amati relation (Amati et al. 2002), consistent with the best estimate value using the BAT spectral slope. Given the low redshift and the prompt emission properties for GRB 080710, it seems thus very likely that $E_{\text{peak}}^{\text{rest}}$ is in a range which is typically associated with a XRR in the GRB rest frame (100-300 keV, Sakamoto et al. 2008), though a hard burst cannot be completely ruled out by the observations.

GROND (Greiner et al. 2008) at the 2.2 m MPI/ESO telescope at LaSilla observatory responded to the *Swift* trigger and initiated automated observations which started 384 s after the burst. During the first two hours only the $g'r'i'z'$ CCDs of GROND were operating. Observations in all seven colors $g'r'i'z'JHK_S$ simultaneously started 1.98 h later and continued until the start of the local nautical twilight at 10:27 UT. Afterwards, GROND switched to a NIR-only mode, where only imaging in JHK_S was performed. TLS imaging was obtained between 00:09 UT and 01:43 UT on 11 July 2008 in filters BVR and I (Schulze et al. 2008). In addition, GROND imaged the field of GRB 080710 3 and 4 days after the burst.

The XRT light curve was downloaded from the XRT light curve repository (Evans et al. 2007) and spectra were obtained with the *xrtpipeline* tool using the latest calibration frames from the *Swift* CALDB and standard parameters. The spectra were fitted using the XSPEC package (Arnaud 1996) with a foreground hydrogen column density at the Galactic value of

$N_{\text{H}}=4.1 \times 10^{20} \text{ cm}^{-2}$ (Kalberla et al. 2005). Optical/NIR data (see Tab. 1 and 2) were reduced using standard IRAF tasks (Tody 1993) similar to the procedure outlined in Krühler et al. (2008).

3. Results

3.1. Afterglow light curve

The optical light curve (Fig. 1) exhibits two salient features during the observation. First, it shows an initial rise in brightness up to a peak at around 2000 s, and second, there is a break in the light curve at roughly 10 ks.

The light curve was parametrized with an empirical model of three smoothly connected power laws. The global χ^2 of $F_{\nu, i}(t)$, where i denotes the individual filter or bandpass, was minimized by assuming an achromatic functional form of $F_{\nu, i}(t) = \eta_{\nu, i} \times F_{\nu}(t)$ where only the overall flux normalization $\eta_{\nu, i}$ depends on the filter. $F_{\nu}(t)$ was adapted from Liang et al. (2008). As a result of the high precision of the data and good sampling in time domain, all parameters were left free to vary and are presented in Tab. 3. In principle, all fit parameters depend on the choice of T_0 . Setting T_0 to the time of the precursor (i.e. -120 s), we find that the fit parameters describing the early/late power laws vary by a maximum of 20% and 2%, respectively. Hence, the uncertainty in T_0 does not change the obtained results significantly or affect the overall conclusions.

Given that the decay after the peak at 2 ks with an index of -0.63 ± 0.02 is too shallow to be explained as the normal decay phase and the late temporal slope of -1.57 ± 0.01 is roughly consistent with the closure relations for the normal decay in the $\nu_m < \nu < \nu_c$ regime for a homogeneous ISM and slow cooling case ($\alpha=3\beta/2$), there is no apparent evidence for a jet-break before 350 ks, and thus $\theta_{\text{jet}} > 10^\circ$ according to Sari et al. (1999).

3.2. Broad-band spectrum

Using the optical/NIR and X-ray data, the afterglow spectrum can be constrained over a broad wavelength range. Four different time intervals were selected to construct a broad band spectral energy distribution (SED, Fig. 2). The different epochs are indicated in the light curve plot with shaded regions, and the SED fit parameters are presented in Tab. 4.

As already indicated by the light curve, there is no sign of spectral evolution throughout the observation. Both the early turnover from rising to falling, as well as the second break are achromatic with high measurement accuracy. The optical/NIR SED alone is consistent with a power law of the X-ray spectral index without strong signatures of curvature due to intrinsic reddening. The expected Galactic foreground extinction $A_V=0.23 \text{ mag}$ (Schlegel et al. 1998) however is significant, so some amount of host extinction might be masked by the uncertainty in the foreground correction. In addition, the obtained optical data hardly probe the rest frame UV regime, where most of any intrinsic extinction would be apparent.

Given that the light curve evolution is similar in both energy ranges and the extrapolation of the X-ray data nicely matches the optical flux, i.e. $\beta_{\text{opt}} \sim \beta_{\text{ox}} \sim \beta_x$, both the optical/NIR and X-ray emission probe the same segment of the afterglow synchrotron spectrum. This implies that the X-ray and optical data are above the typical synchrotron frequency ν_m and in the spectral regime of $\max(\nu_m, \nu_c) < \nu_{\text{opt}} < \nu_X$, or $\nu_m < \nu_{\text{opt}} < \nu_X < \nu_c$, where the latter is consistent with fireball model in a homogeneous ISM and slow cooling case. The spectral index of the electron distribution

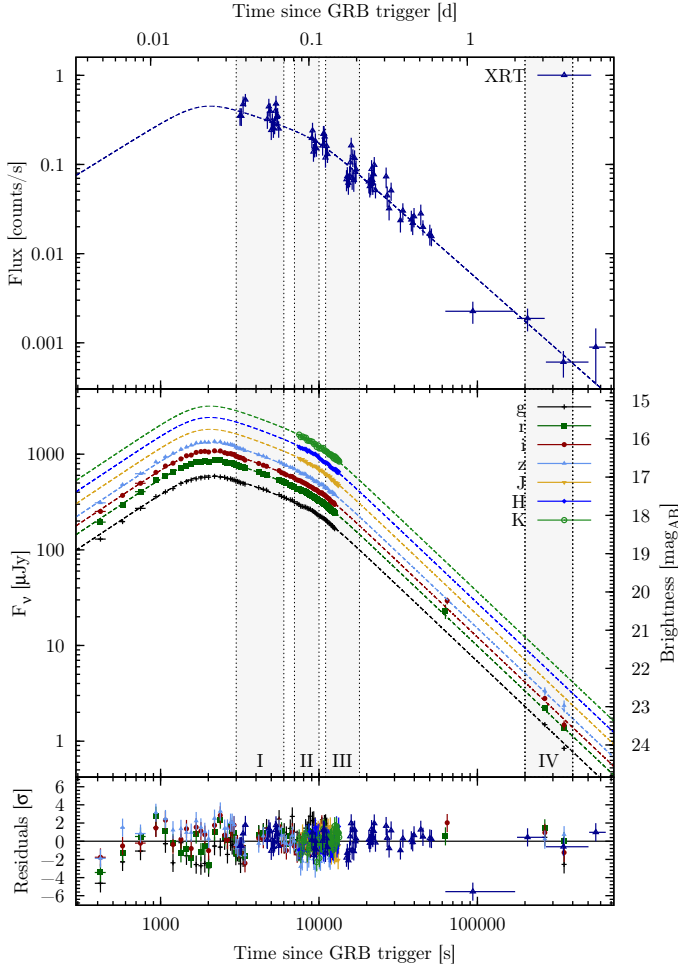


Fig. 1. Light curves of the X-ray (top panel) and optical/NIR (middle panel) afterglow of GRB 080710. Residuals to the combined light curve fit are shown in the lowest panel. Shown data are not corrected for Galactic foreground reddening. Upper limits are not shown to enhance clarity.

p would then be $p=2\beta=2.00\pm 0.02$ or $2\beta+1=3.00\pm 0.02$, respectively. Given that not all bursts are consistent with the closure relations in the basic fireball scenario (e.g. Evans et al. 2008), we consider both cases in the following. Consequentially, the expected break in the synchrotron afterglow spectrum at the cooling frequency ν_c could be below the optical at the start of the observations 6 minutes after the burst, or, assuming $\nu_m < \nu < \nu_c$, above the X-rays for the whole observational period.

4. Discussion

A number of previous bursts have shown a rising optical afterglow at early times, e.g. GRBs 060418, 060607A (Molinari et al. 2007) amongst others (e.g. Krühler et al. 2008; Ferrero et al. 2009; Greiner et al. 2009b; Oates et al. 2009; Rykoff et al. 2009; Klotz et al. 2009). Similar to the X-Ray Flash 071031 (Krühler et al. 2009), the optical SED does not show significant evolution during the rise, and all bands peak at the same time.

An achromatic rising component is generally related to either the onset of the fireball forward shock (e.g. Sari et al. 1999) seen face-on, or to an outflow seen off-axis (e.g. Panaitescu et al. 1998). In the first case, the apparent increase in brightness is caused by the increasing number of radiating electrons. The time

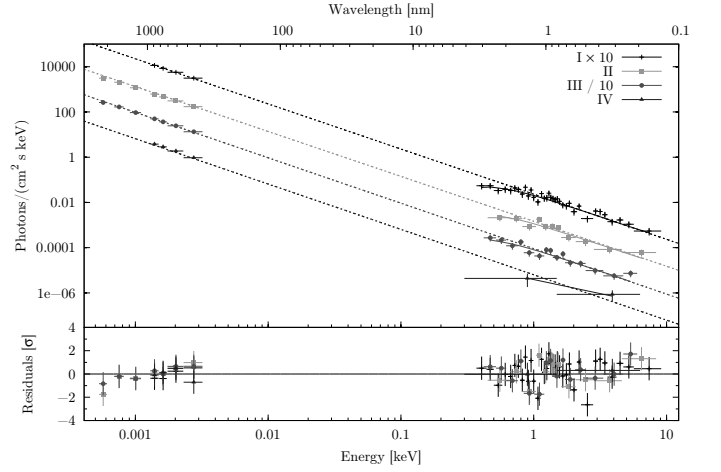


Fig. 2. Broad band spectral energy distribution from XRT and GROND at different epochs (upper panel). The data were fitted with a power-law, modified by a Galactic and intrinsic hydrogen column. The best fit power law is shown in dotted lines, the best fit model including the soft X-ray absorption in solid lines. In the lower panel the residuals of the data to the best fit model.

of the light curve peak at T_0+2 ks is much later than the end of significant γ emission (T_0+40 s), so the afterglow can be described in the thin shell approximation. The jet is then expected to produce a peak in the light curve when the swept up circumburst medium efficiently decelerates the ejecta. Depending on the profile of the circumburst medium, the rise has indices of ~ 2 ($\nu_c < \nu_{\text{opt}}$) or 3 ($\nu_c > \nu_{\text{opt}}$) in an ISM, or ~ 0.5 in a wind environment (Panaitescu & Vestrand 2008). Given that the majority of bursts prefer an ISM profile, and the late afterglow decline is consistent with it, we thus consider only the ISM thin shell case in the following.

In the off-axis case the peak is a geometric effect: as the shock wave decelerates, the relativistically beamed emission cone widens and gradually enters the sight line of the observer. The light curve morphology is then dependent on the jet's structure and off axis angle θ_{obs} , and reaches a maximum when $\Gamma \sim (\theta_{\text{obs}} - \theta_c)^{-1}$ where θ_c is the angle of a uniform cone around the symmetry axis of the jet.

There is no evidence of chromatic evolution, which would be the case if the peak was caused by a moving ν_m through the optical bands or dust destruction, and none of these processes produce the early rise. In addition, there is also no sign of a reverse shock, which is expected to decline with a temporal index of -1.75 for $p=2$ or -2.5 for $p=3$. The latter, however, might be masked by a dominating forward shock, or happened before the start of the GROND observations.

4.1. Decelerating ejecta in an on-axis geometry

If the light curve peak was caused by a jet in its pre deceleration phase, conclusions about the motion of the ultra-relativistic outflow from the central engine can be drawn. Using the time of the absolute light curve maximum $t_{\text{max}} \approx 2$ ks, $\log E_{\gamma, \text{iso}} [\text{erg}] = 51.70-52.14$ and following Molinari et al. (2007), we find initial Lorentz factors of the bulk outflow of around $\Gamma_0^{\text{ISM}} \approx 90-100$ ($\Gamma_0^{\text{wind}} \approx 30-40$). This is at the very low end of the theoretically expected velocity of the outflow to produce γ -rays (e.g. Piran 2005), and together with the divergence in the measured (1.1) and expected ($\sim 2-3$) rise index, makes the scenario of a single

on-axis decelerating jet somewhat contrived. In addition, there seems to be a small population of late-peaking afterglows or long plateaus (e.g. XRF 030723 (Fynbo et al. 2004) or GRB 060614 (Della Valle et al. 2006)) where the derived Lorentz-factor in an on-axis geometry from the optical afterglow peak are uncomfortably small. Furthermore, all previously observed rise indices have a broad distribution (cp. e.g. Panaitescu & Vestrand (2008); Oates et al. (2009); Rykoff et al. (2009); Klotz et al. (2009) and references therein) from early plateaus to very fast rising curves, and they do not cluster around the expected t^{2-3} . Consequentially, it seems plausible that at least some rising afterglows are not caused by the onset of the afterglow, but rather by a geometrical offset of the observers sight line with respect to the jets central cone.

4.2. Jet seen off-axis

Contrary to the model of an on-axis jet in its pre deceleration phase, an off-axis scenario is able to account for a broad range of observed rise indices. The peak time and rise index then relates to the off-axis angle or jet structure and therefore could describe a large diversity of early afterglows in a single framework (Panaitescu & Vestrand 2008).

If the energy in the jet outer wings decreases rapidly, the early emission of the line of sight ejecta is negligible as compared to the central part, and the jet structure can be approximated as a homogeneous top-hat, where the burst energetics can be used to constrain the offset angle. Following Granot et al. (2002), a homogeneous jet with a half opening angle θ_{jet} and a Lorentz factor Γ seen off-axis at an angle θ_{obs} will appear less energetic by a factor of b^6 , where $b = \Gamma(\theta_{\text{obs}} - \theta_{\text{jet}})$. Assuming a mean value of $\log E_{\gamma, \text{iso}} [\text{erg}] = 53$ and, hence adopting $b^6 \lesssim 10$ for GRB 080710, it follows $\theta_{\text{obs}} - \theta_{\text{jet}} \lesssim 3^\circ / \Gamma_{100} \cdot E_{\text{peak}}^{\text{obs}}$, if viewed on-axis, would then be $b^2 E_{\text{peak}}^{\text{obs}} \approx 300 \text{ keV}$.

However, the jet geometry does not necessarily have to be a simple top-hat. In a realistic jet model, the jet viewed off-axis is inhomogeneous, i.e. has a top-hat structure with wings of lower energy, or is Gaussian shaped (e.g. Zhang et al. 2003; Eichler & Granot 2006). In addition, some bursts show evidence that their jet structure is a composition of two jets (Berger et al. 2003; Granot et al. 2006; Racusin et al. 2008). In this two component jet model a narrow, fast jet produces the γ -rays and early afterglow, and a slow wide jet dominates the late afterglow emission (Peng et al. 2005).

In these cases, the resulting afterglow light curve in an off-axis geometry is a superposition of two different components: the emission from the ejecta with lower Lorentz-factors, typically dominating at late times, and the relativistic spreading of the decelerating jet around the symmetry axis. The relative energies, jet structure and offset angle then define the light curve morphology. In particular, the delayed onset of the broad jet emission in its pre deceleration phase might be responsible for the shallow decay observed after the peak. Remarkably, the light curve is equally well ($\chi^2=485$ for 425 d.o.f) fit using the sum of the afterglow of two jets, where the narrow one is viewed slightly off-axis (Fig. 3). Hence, the shallow decay phase could be the result of the superposition of the normal decay phase of the narrow-jet afterglow and the rise of the broad jet with $\Gamma_0 \sim 50$, $\theta_{\text{jet}} > 10^\circ$ in its pre deceleration phase. After the emergence of the broad jet afterglow, it subsequently dominates the light curve morphology (Fig. 3). The two component model thus provides a phenomenological explanation for the shallow decay phase by attributing the shallow slope to the increasing energy

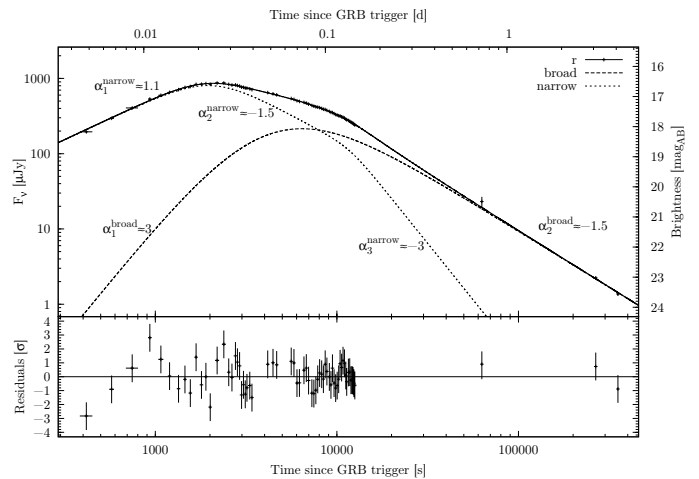


Fig. 3. Two component fit for GRB 080710 as the superposition of the afterglow of two jets with $v_m < v_{\text{opt}} < v_X < v_c$ and $p \sim 3$ for both components. The narrow jet is viewed slightly off-axis and produces a shallow rise as its emission spreads during deceleration due to relativistic beaming effects. The broad jet is viewed on-axis with $\Gamma_0 \sim 50$, $\theta_{\text{jet}} > 10^\circ$ and has the expected steep rise during its pre deceleration phase. Shown is the GROND r' band data, all other bands are omitted to enhance clarity.

dissipation in the pre deceleration phase of the broader jet in a specific jet configuration. The opening angle of the narrow jet can be constrained from the light curve fitting to around $2-4^\circ$, but its jet break is masked by the brighter broad jet at later times (Fig. 3). An alternative, jet geometry independent mechanism of energy injection during the shallow decay phase is the refreshed shock scenario (e.g. Rees & Meszaros 1998; Zhang et al. 2006). A long lived central engine or a simultaneous ejection of shells with a distribution of Lorentz factors could cause the continuous energy injection required for a shallow decay (e.g. Nousek et al. 2006).

An off-axis viewing angle in a two component or structured jet model with an energy injection can thus provide a consistent picture for the light curve morphology and the relatively low estimates of $E_{\gamma, \text{iso}}$ and $E_{\text{peak}}^{\text{rest}}$ of the prompt emission of GRB 080710. In an off-axis scenario, a lower $E_{\text{peak}}^{\text{rest}}$ of the prompt emission spectrum would correspond to a later and fainter afterglow maximum, as both are caused by geometric effects. We caution that the spectral properties of BAT bursts are generally not well constrained, and GRB 080710 is no exception in this aspect. The BAT data, however, indicate a mildly soft event, which could be associated with a XRR in the bursts restframe, consistent with the off-axis interpretation of the optical light curve in a unified model.

5. Conclusions

The broad-band light curve of the afterglow of GRB 080710 shows two salient features, both achromatic with high precision: an early rise in its brightness, peaking at ~ 2 ks, and a turnover from a shallow to steep decline at ~ 10 ks. The early rise can be caused by a jet in its pre deceleration phase, or a viewing angle outside the central cone. The latter scenario is naturally able to explain a late-rising afterglow for a soft and weak burst due to a viewing angle offset with respect to the symmetry axis of the jet. An off-axis scenario provides a consistent description of the properties of GRB 080710, and can additionally ac-

count for a broad range of rise indices. Consequentially, some of the rising afterglow light curves, especially late and shallow ones, might not represent the same class of afterglows which rise due to increasing emission in the pre deceleration phase, but rather provide evidence for an off-axis location of the observer. The achromatic early increase in brightness observed in the mildly soft GRB 080710 is too shallow to be accounted for with the onset of the afterglow, but significantly steeper than recently observed in the XRFs 071031 (Krühler et al. 2009) and 080330 (Guidorzi et al. 2009). This might already hint on a common dependence of $E_{\text{peak}}^{\text{rest}}$ and the rise index of the early optical light curve on the off-axis angle as expected in a unified model: the softer the prompt emission, the more off-axis, and thus the shallower the rise. It remains to be tested with a larger sample of early afterglows with well constrained energetics and light curves of the prompt emission from combined *Swift*/BAT and *Fermi*/GBM detections, whether and how the structure of an early rise in the optical afterglow is related to prompt emission properties, and in particular, the rest frame $E_{\text{peak}}^{\text{rest}}$ and $E_{\gamma, \text{iso}}$. A possible correlation would then shed light on the nature of the early afterglow rise, the shallow decay segment, and the jet structure in general.

Acknowledgements. We thank the referee for very helpful comments, which helped to increase the quality of the paper significantly. TK acknowledges support by the DFG cluster of excellence 'Origin and Structure of the Universe'. A.R. and S.K. acknowledge support by DFG grant Kl 766/11-3. Part of the funding for GROND (both hardware and personnel) was granted from the Leibniz-Prize to Prof. G. Hasinger (DFG grant HA 1850/28-1). SS acknowledges support by a Grant of Excellence from the Icelandic Research Fund. This work made use of data supplied by the UK Swift Science Data Centre at the University of Leicester.

References

- Abdo, A. A., Ackermann, M., & Arimoto, M. 2009, *Science*, 1688
- Amati, L., Frontera, F., Tavani, M., et al. 2002, *A&A*, 390, 81
- Amati, L., Guidorzi, C., Frontera, F., et al. 2008, *MNRAS*, 391, 577
- Arnaud, K. A. 1996, in *ASPC Ser.*, Vol. 101, *Astronomical Data Analysis Software and Systems V*, ed. G. H. Jacoby & J. Barnes, 17
- Band, D., Matteson, J., Ford, L., et al. 1993, *ApJ*, 413, 281
- Barthelmy, S. D. et al. 2005, *Space Science Reviews*, 120, 143
- Berger, E., Kulkarni, S. R., Pooley, G., et al. 2003, *Nature*, 426, 154
- Burrows, D. N. et al. 2005, *Space Science Reviews*, 120, 165
- Della Valle, M., Chincarini, G., Panagia, N., et al. 2006, *Nature*, 444, 1050
- Eichler, D. & Granot, J. 2006, *ApJ*, 641, L5
- Evans, P. A., Beardmore, A. P., Page, K. L., et al. 2008, *ArXiv:0812.3662*
- Evans, P. A. et al. 2007, *A&A*, 469, 379
- Ferrero, P. et al. 2009, *A&A*, 497, 729
- Fynbo, J. P. U., Jakobsson, P., Prochaska, J. X., et al. 2009, *ArXiv:0907.3449*
- Fynbo, J. P. U., Sollerman, J., Hjorth, J., et al. 2004, *ApJ*, 609, 962
- Gehrels, N. et al. 2004, *ApJ*, 611, 1005
- Granot, J., Königl, A., & Piran, T. 2006, *MNRAS*, 370, 1946
- Granot, J. & Kumar, P. 2003, *ApJ*, 591, 1086
- Granot, J., Panaitescu, A., Kumar, P., & Woosley, S. E. 2002, *ApJ*, 570, L61
- Greiner, J., Bornemann, W., Clemens, C., et al. 2008, *PASP*, 120, 405
- Greiner, J., Clemens, C., Krühler, T., et al. 2009a, *A&A*, 498, 89
- Greiner, J., Krühler, T., McBreen, S., et al. 2009b, *ApJ*, 693, 1912
- Guidorzi, C., Clemens, C., Kobayashi, S., et al. 2009, *A&A*, 499, 439
- Heise, J., in 't Zand, J., Kippen, R. M., & Woods, P. M. 2001, in *Gamma-ray Bursts in the Afterglow Era*, ed. E. Costa, F. Frontera, & J. Hjorth, 16
- Kalberla, P. M. W., Burton, W. B., Hartmann, D., et al. 2005, *A&A*, 440, 775
- Kippen, R. M., Woods, P. M., Heise, J., et al. 2003, in *AIPC*, Vol. 662, *Gamma-Ray Burst and Afterglow Astronomy 2001*, ed. G. R. Ricker & R. K. Vanderspek, 244
- Klotz, A., Boër, M., Atteia, J. L., & Gendre, B. 2009, *AJ*, 137, 4100
- Krühler, T., Greiner, J., McBreen, S., et al. 2009, *ApJ*, 697, 758
- Krühler, T., Küpcü Yoldaş, A., Greiner, J., et al. 2008, *ApJ*, 685, 376
- Kumar, P. & Granot, J. 2003, *ApJ*, 591, 1075
- Lamb, D. Q., Donaghy, T. Q., & Graziani, C. 2005, *ApJ*, 620, 355
- Landsman, W. B. & Sbarufatti, B. 2008, *GCN*, 7965
- Liang, E.-W., Racusin, J. L., Zhang, B., Zhang, B.-B., & Burrows, D. N. 2008, *ApJ*, 675, 528
- Mészáros, P., Rees, M. J., & Wijers, R. A. M. J. 1998, *ApJ*, 499, 301
- Molinari, E., Vergani, S. D., Malesani, D., et al. 2007, *A&A*, 469, L13
- Nousek, J. A., Kouveliotou, C., Grupe, D., et al. 2006, *ApJ*, 642, 389
- Oates, S. R., Page, M. J., Schady, P., et al. 2009, *MNRAS*, 395, 490
- Panaitescu, A., Mészáros, P., & Rees, M. J. 1998, *ApJ*, 503, 314
- Panaitescu, A. & Vestrand, W. T. 2008, *MNRAS*, 387, 497
- Peng, F., Königl, A., & Granot, J. 2005, *ApJ*, 626, 966
- Perley, D. A., Chornock, R., & Bloom, J. S. 2008, *GCN*, 7962
- Piran, T. 2005, *Reviews of Modern Physics*, 76, 1143
- Preece, R. D., Briggs, M. S., Malozzi, R. S., et al. 2000, *ApJS*, 126, 19
- Racusin, J. L., Karpov, S. V., Sokolowski, M., et al. 2008, *Nature*, 455, 183
- Rees, M. J. & Meszaros, P. 1998, *ApJ*, 496, L1+
- Rhoads, J. E. 1999, *ApJ*, 525, 737
- Roming, P. W. A. et al. 2005, *Space Science Reviews*, 120, 95
- Rossi, E., Lazzati, D., & Rees, M. J. 2002, *MNRAS*, 332, 945
- Rykoff, E. S., Aharonian, F., Akerlof, C. W., et al. 2009, *ArXiv:0904.0261*
- Sakamoto, T., Hullinger, D., Sato, G., et al. 2008, *ApJ*, 679, 570
- Sakamoto, T., Lamb, D. Q., Kawai, N., et al. 2005, *ApJ*, 629, 311
- Sakamoto, T., Sato, G., Barbier, L., et al. 2009, *ApJ*, 693, 922
- Sari, R., Piran, T., & Halpern, J. P. 1999, *ApJ*, 519, L17
- Sbarufatti, B., Baumgartner, W. H., Evans, P. A., et al. 2008, *GCN*, 7957
- Schlegel, D. J., Finkbeiner, D. P., & Davis, M. 1998, *ApJ*, 500, 525
- Schulze, S., Kann, D. A., Rossi, A., et al. 2008, *GCN*, 7972
- Tody, D. 1993, in *ASPC Ser.*, Vol. 52, *Astronomical Data Analysis Software and Systems II*, ed. R. J. Hanisch, R. J. V. Brissenden, & J. Barnes, 173
- Tueller, J., Barthelmy, S. D., Baumgartner, W., et al. 2008, *GCN*, 7969
- Woods, E. & Loeb, A. 1999, *ApJ*, 523, 187
- Yamazaki, R., Ioka, K., & Nakamura, T. 2002, *ApJ*, 571, L31
- Zhang, B., Fan, Y. Z., Dyks, J., et al. 2006, *ApJ*, 642, 354
- Zhang, B. & Mészáros, P. 2002, *ApJ*, 571, 876
- Zhang, W., Woosley, S. E., & MacFadyen, A. I. 2003, *ApJ*, 586, 356

Online Material

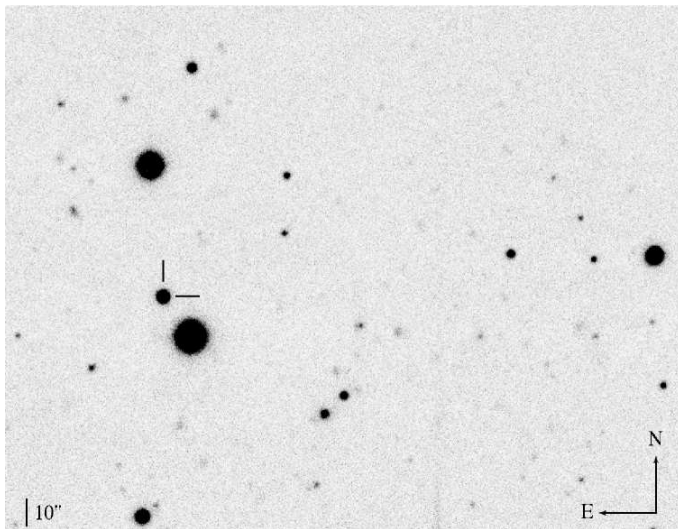


Fig. 1. GROND r' band image of the field of GRB 080710 obtained approximately 2 ks after T_0 . The optical afterglow is marked and the shown image is roughly 4.2' by 3.2'.

Table 1. griz photometric data

$T_{\text{mid}} - T_0$ [ks]	Exposure [s]	Filter	Brightness ^(a)			
			g'	r'	i'	z'
0.4169	66	$g'r'iz'$	18.619 ± 0.028	18.175 ± 0.026	17.899 ± 0.026	17.673 ± 0.028
0.5745	35	$g'r'iz'$	18.162 ± 0.024	17.724 ± 0.018	17.478 ± 0.018	17.200 ± 0.019
0.7457	115	$g'r'iz'$	17.815 ± 0.016	17.381 ± 0.010	17.162 ± 0.015	16.909 ± 0.016
0.9334	35	$g'r'iz'$	17.509 ± 0.013	17.086 ± 0.009	16.875 ± 0.011	16.604 ± 0.016
1.0726	71	$g'r'iz'$	17.385 ± 0.008	16.961 ± 0.006	16.711 ± 0.009	16.474 ± 0.011
1.1977	35	$g'r'iz'$	17.300 ± 0.008	16.865 ± 0.006	16.637 ± 0.008	16.381 ± 0.009
1.3423	35	$g'r'iz'$	17.163 ± 0.007	16.773 ± 0.006	16.523 ± 0.007	16.274 ± 0.008
1.4556	35	$g'r'iz'$	17.118 ± 0.007	16.701 ± 0.005	16.442 ± 0.007	16.215 ± 0.007
1.5595	35	$g'r'iz'$	17.075 ± 0.007	16.668 ± 0.005	16.425 ± 0.007	16.169 ± 0.007
1.6767	35	$g'r'iz'$	17.044 ± 0.006	16.596 ± 0.005	16.354 ± 0.007	16.112 ± 0.007
1.7947	35	$g'r'iz'$	17.020 ± 0.006	16.595 ± 0.005	16.334 ± 0.007	16.095 ± 0.008
1.8996	35	$g'r'iz'$	17.003 ± 0.006	16.573 ± 0.005	16.326 ± 0.007	16.089 ± 0.007
2.0065	35	$g'r'iz'$	17.003 ± 0.006	16.593 ± 0.005	16.343 ± 0.006	16.094 ± 0.006
2.1892	115	$g'r'iz'$	16.976 ± 0.005	16.552 ± 0.004	16.312 ± 0.004	16.070 ± 0.005
2.3835	115	$g'r'iz'$	16.995 ± 0.005	16.553 ± 0.004	16.315 ± 0.004	16.078 ± 0.005
2.5359	35	$g'r'iz'$	17.007 ± 0.006	16.597 ± 0.004	16.363 ± 0.007	16.121 ± 0.006
2.6421	35	$g'r'iz'$	17.042 ± 0.006	16.617 ± 0.005	16.386 ± 0.007	16.136 ± 0.007
2.7614	35	$g'r'iz'$	17.044 ± 0.006	16.617 ± 0.005	16.387 ± 0.006	16.147 ± 0.007
2.8323	35	$g'r'iz'$	17.061 ± 0.006	16.635 ± 0.005	16.401 ± 0.007	16.159 ± 0.007
2.9105	35	$g'r'iz'$	17.074 ± 0.006	16.652 ± 0.005	16.409 ± 0.007	16.176 ± 0.007
2.9854	35	$g'r'iz'$	17.103 ± 0.006	16.692 ± 0.005	16.453 ± 0.007	16.219 ± 0.007
3.0564	35	$g'r'iz'$	17.110 ± 0.006	16.696 ± 0.005	16.463 ± 0.007	16.236 ± 0.007
3.1276	35	$g'r'iz'$	17.125 ± 0.007	16.718 ± 0.005	16.483 ± 0.007	16.248 ± 0.008
3.1962	35	$g'r'iz'$	17.151 ± 0.006	16.724 ± 0.005	16.492 ± 0.007	16.261 ± 0.008
3.3151	35	$g'r'iz'$	17.164 ± 0.006	16.744 ± 0.005	16.513 ± 0.007	16.273 ± 0.008
3.4059	35	$g'r'iz'$	17.181 ± 0.007	16.771 ± 0.005	16.554 ± 0.008	16.309 ± 0.007
4.1611	115	$g'r'iz'$	17.273 ± 0.005	16.869 ± 0.004	16.643 ± 0.005	16.418 ± 0.006
4.4496	115	$g'r'iz'$	17.315 ± 0.005	16.911 ± 0.004	16.689 ± 0.005	16.452 ± 0.006
4.6632	115	$g'r'iz'$	17.341 ± 0.005	16.944 ± 0.004	16.716 ± 0.005	16.488 ± 0.006
5.6014	115	$g'r'iz'$	17.456 ± 0.005	17.067 ± 0.004	16.830 ± 0.005	16.601 ± 0.006
5.8030	115	$g'r'iz'$	17.501 ± 0.006	17.094 ± 0.004	16.881 ± 0.006	16.637 ± 0.006
6.0290	115	$g'r'iz'$	17.529 ± 0.005	17.140 ± 0.004	16.910 ± 0.006	16.675 ± 0.006
6.2166	115	$g'r'iz'$	17.556 ± 0.006	17.163 ± 0.004	16.941 ± 0.005	16.700 ± 0.006
6.5862	115	$g'r'iz'$	17.591 ± 0.006	17.197 ± 0.004	16.977 ± 0.006	16.746 ± 0.006
6.7883	115	$g'r'iz'$	17.598 ± 0.006	17.219 ± 0.004	16.984 ± 0.006	16.757 ± 0.006
6.9845	115	$g'r'iz'$	17.643 ± 0.006	17.254 ± 0.004	17.028 ± 0.006	16.788 ± 0.007
7.2804	115	$g'r'iz'$	17.689 ± 0.006	17.300 ± 0.004	17.073 ± 0.006	16.839 ± 0.007
7.4691	115	$g'r'iz'$	17.713 ± 0.006	17.323 ± 0.004	17.087 ± 0.006	16.853 ± 0.006
7.6567	115	$g'r'iz'$	17.760 ± 0.005	17.342 ± 0.004	17.101 ± 0.004	16.902 ± 0.006
7.8462	115	$g'r'iz'$	17.769 ± 0.005	17.355 ± 0.004	17.130 ± 0.005	16.918 ± 0.006
8.0363	115	$g'r'iz'$	17.779 ± 0.004	17.371 ± 0.004	17.150 ± 0.005	16.918 ± 0.006
8.2434	115	$g'r'iz'$	17.786 ± 0.006	17.397 ± 0.004	17.170 ± 0.007	16.928 ± 0.007
8.4312	115	$g'r'iz'$	17.812 ± 0.005	17.423 ± 0.004	17.197 ± 0.005	16.989 ± 0.007
8.6219	115	$g'r'iz'$	17.826 ± 0.004	17.432 ± 0.004	17.226 ± 0.004	17.005 ± 0.006
8.8119	115	$g'r'iz'$	17.836 ± 0.006	17.461 ± 0.005	17.247 ± 0.005	17.010 ± 0.006
9.0840	115	$g'r'iz'$	17.875 ± 0.006	17.498 ± 0.005	17.274 ± 0.008	17.043 ± 0.010
9.2723	115	$g'r'iz'$	17.898 ± 0.006	17.527 ± 0.004	17.304 ± 0.006	17.086 ± 0.007
9.4591	115	$g'r'iz'$	17.929 ± 0.005	17.534 ± 0.004	17.324 ± 0.006	17.123 ± 0.008
9.6457	115	$g'r'iz'$	17.960 ± 0.005	17.570 ± 0.004	17.333 ± 0.005	17.116 ± 0.006
9.8478	115	$g'r'iz'$	17.989 ± 0.006	17.599 ± 0.005	17.366 ± 0.007	17.132 ± 0.008
10.037	115	$g'r'iz'$	18.013 ± 0.005	17.619 ± 0.004	17.401 ± 0.005	17.180 ± 0.006
10.227	115	$g'r'iz'$	18.025 ± 0.005	17.636 ± 0.004	17.419 ± 0.005	17.206 ± 0.007
10.420	115	$g'r'iz'$	18.046 ± 0.006	17.646 ± 0.005	17.408 ± 0.004	17.187 ± 0.008
10.622	115	$g'r'iz'$	18.072 ± 0.006	17.674 ± 0.005	17.446 ± 0.007	17.203 ± 0.008
10.811	115	$g'r'iz'$	18.091 ± 0.005	17.692 ± 0.004	17.467 ± 0.005	17.266 ± 0.006
11.001	115	$g'r'iz'$	18.114 ± 0.005	17.718 ± 0.004	17.494 ± 0.005	17.281 ± 0.006
11.194	115	$g'r'iz'$	18.142 ± 0.005	17.753 ± 0.007	17.523 ± 0.006	17.289 ± 0.006
11.333	115	$g'r'iz'$	18.175 ± 0.006	17.776 ± 0.004	17.547 ± 0.007	17.302 ± 0.008
11.574	115	$g'r'iz'$	18.199 ± 0.005	17.798 ± 0.005	17.567 ± 0.008	17.365 ± 0.006
11.763	115	$g'r'iz'$	18.222 ± 0.005	17.822 ± 0.004	17.613 ± 0.008	17.391 ± 0.006
11.957	115	$g'r'iz'$	18.258 ± 0.006	17.855 ± 0.009	17.633 ± 0.008	17.400 ± 0.007
12.134	66	$g'r'iz'$	18.268 ± 0.011	17.877 ± 0.007	17.656 ± 0.010	17.395 ± 0.010
12.270	66	$g'r'iz'$	18.300 ± 0.007	17.895 ± 0.005	17.671 ± 0.007	17.415 ± 0.010
12.410	66	$g'r'iz'$	18.320 ± 0.011	17.915 ± 0.006	17.671 ± 0.009	17.462 ± 0.010
12.552	66	$g'r'iz'$	18.348 ± 0.013	17.948 ± 0.008	17.714 ± 0.011	17.443 ± 0.013
62.856	300	$R^{(d)}$		20.49 ± 0.18		
64.523	4 x 300	$I^{(d)}$		20.23 ± 0.09		
266.59	8 x 365	$g'r'iz'$	23.47 ± 0.06	23.02 ± 0.05	22.79 ± 0.07	22.59 ± 0.11

Table 2. JHK_S photometric data

$T_{\text{mid}} - T_0$ [ks]	Exposure [s] [s]	Filter	Brightness ^(a) mag _{AB} ^(bc)		
7.4943	12 x 10	JHK _S	16.506 ± 0.009	16.215 ± 0.017	15.887 ± 0.019
7.6818	12 x 10	JHK _S	16.541 ± 0.008	16.240 ± 0.017	15.954 ± 0.019
7.8710	12 x 10	JHK _S	16.533 ± 0.008	16.251 ± 0.011	15.940 ± 0.013
8.0611	12 x 10	JHK _S	16.571 ± 0.008	16.264 ± 0.013	15.962 ± 0.014
8.2685	12 x 10	JHK _S	16.591 ± 0.009	16.267 ± 0.012	15.968 ± 0.014
8.4560	12 x 10	JHK _S	16.638 ± 0.008	16.329 ± 0.015	16.042 ± 0.016
8.6469	12 x 10	JHK _S	16.638 ± 0.008	16.309 ± 0.012	16.052 ± 0.014
8.8370	12 x 10	JHK _S	16.664 ± 0.009	16.346 ± 0.013	16.058 ± 0.015
9.1091	12 x 10	JHK _S	16.703 ± 0.009	16.378 ± 0.014	16.075 ± 0.016
9.2966	12 x 10	JHK _S	16.706 ± 0.008	16.397 ± 0.011	16.135 ± 0.013
9.4841	12 x 10	JHK _S	16.714 ± 0.008	16.397 ± 0.013	16.140 ± 0.015
9.6707	12 x 10	JHK _S	16.745 ± 0.009	16.437 ± 0.012	16.215 ± 0.014
9.8729	12 x 10	JHK _S	16.765 ± 0.009	16.455 ± 0.017	16.175 ± 0.018
10.062	12 x 10	JHK _S	16.825 ± 0.009	16.508 ± 0.015	16.252 ± 0.016
10.252	12 x 10	JHK _S	16.810 ± 0.008	16.533 ± 0.016	16.231 ± 0.017
10.447	12 x 10	JHK _S	16.842 ± 0.008	16.556 ± 0.017	16.258 ± 0.018
10.646	12 x 10	JHK _S	16.857 ± 0.009	16.599 ± 0.017	16.236 ± 0.018
10.835	12 x 10	JHK _S	16.908 ± 0.008	16.611 ± 0.017	16.310 ± 0.019
11.025	12 x 10	JHK _S	16.916 ± 0.008	16.620 ± 0.015	16.321 ± 0.016
11.213	12 x 10	JHK _S	16.949 ± 0.009	16.629 ± 0.014	16.334 ± 0.016
11.415	12 x 10	JHK _S	16.950 ± 0.009	16.658 ± 0.014	16.370 ± 0.016
11.598	12 x 10	JHK _S	16.989 ± 0.009	16.684 ± 0.011	16.411 ± 0.013
11.788	12 x 10	JHK _S	16.993 ± 0.008	16.737 ± 0.012	16.405 ± 0.014
11.983	12 x 10	JHK _S	17.071 ± 0.009	16.751 ± 0.013	16.414 ± 0.015
12.140	6 x 10	JHK _S	17.048 ± 0.011	16.770 ± 0.013	16.465 ± 0.014
12.277	6 x 10	JHK _S	17.079 ± 0.011	16.794 ± 0.014	16.453 ± 0.016
12.417	6 x 10	JHK _S	17.099 ± 0.010	16.788 ± 0.016	16.512 ± 0.017
12.560	6 x 10	JHK _S	17.141 ± 0.011	16.805 ± 0.016	16.458 ± 0.017
12.707	6 x 10	JHK _S	17.154 ± 0.010	16.796 ± 0.015	16.478 ± 0.016
12.806	6 x 10	JHK _S	17.144 ± 0.010	16.820 ± 0.014	16.543 ± 0.016
12.904	6 x 10	JHK _S	17.177 ± 0.011	16.808 ± 0.012	16.500 ± 0.014
13.003	6 x 10	JHK _S	17.174 ± 0.011	16.878 ± 0.024	16.553 ± 0.025
13.116	6 x 10	JHK _S	17.170 ± 0.011	16.863 ± 0.015	16.544 ± 0.016
13.209	6 x 10	JHK _S	17.226 ± 0.010	16.887 ± 0.017	16.555 ± 0.018
13.308	6 x 10	JHK _S	17.210 ± 0.010	16.856 ± 0.014	16.569 ± 0.016
13.408	6 x 10	JHK _S	---	16.883 ± 0.019	16.593 ± 0.020
269.07	240 x 10	JHK _S	> 22.47	> 21.97	> 21.224
354.88	240 x 10	JHK _S	> 22.29	> 22.04	> 21.082

^(a) Not corrected for Galactic foreground reddening, but converted to AB magnitudes for consistency with Tab. 1

^(b) In the light curve fitting, a systematic error of 0.02 mag was added quadratically to the quoted statistical error

^(c) For the SED fitting, the additional error of the absolute calibration of 0.07 (J and H) and 0.09 (K) mag was added

Table 3. Light curve fits

Bands	$F_\nu(t)$	$\alpha_r^{(a)}$	s_1	$t_{b,1}$ [s]	$\alpha_{d,1}^{(a)}$	s_2	$t_{b,2}$ [s]	$\alpha_{d,2}^{(a)}$	$\chi^2/\text{d.o.f}$
g'	TPL ^(b)	1.20 ± 0.11	2.2 ± 0.5	1775 ± 62	-0.64 ± 0.04	7.2 ± 1.7	9665 ± 170	-1.58 ± 0.01	58 / 59
r'	TPL ^(b)	1.11 ± 0.07	2.6 ± 0.4	1816 ± 39	-0.65 ± 0.03	6.7 ± 1.3	9767 ± 157	-1.55 ± 0.01	49 / 60
i'	TPL ^(b)	1.10 ± 0.05	3.1 ± 0.5	1836 ± 37	-0.63 ± 0.03	5.5 ± 1.2	9752 ± 185	-1.56 ± 0.02	52 / 60
z'	TPL ^(b)	1.10 ± 0.06	3.4 ± 0.5	1835 ± 34	-0.60 ± 0.04	4.2 ± 1.0	9795 ± 268	-1.56 ± 0.03	61 / 59
JHK	DPL ^(c)	—	—	—	-0.53 ± 0.15	5.7 ± 1.7	9542 ± 527	-1.57 ± 0.15	84 / 99
$g'r'i'z'JHK_S$	TPL ^(b)	1.11 ± 0.03	2.9 ± 0.2	1829 ± 19	-0.63 ± 0.02	5.7 ± 0.5	9763 ± 83	-1.57 ± 0.01	425 / 362
$g'r'i'z'JHK_S + \text{X-ray}$	TPL ^(b)	1.11 ± 0.03	2.9 ± 0.2	1829 ± 19	-0.63 ± 0.02	5.7 ± 0.5	9759 ± 82	-1.57 ± 0.01	488 / 428

^(a) Power law indices α of the segmented light curve, which are connected via breaks with smoothness s at break times t_b

^(b) Smoothly connected triple power law

^(c) Smoothly connected double power law

Table 4. SED fits

Epoch	Spectral index β	$N_{\text{H}}^{(a)}$ [10^{22}cm^{-2}]	$\chi^2/\text{d.o.f}$
I	1.00 ± 0.01	0.19 ± 0.09	36 / 36
II	0.99 ± 0.01	0.17 ± 0.10	15 / 15
III	1.01 ± 0.01	$0.13^{+0.15}_{-0.13}$	18 / 19
IV	1.01 ± 0.01	$0.53^{+1.30}_{-0.53}$	0.3 / 3

^(a) Intrinsic hydrogen column density, in excess of the frozen Galactic foreground of $N_{\text{H}}=4.1 \times 10^{20} \text{cm}^{-2}$